H. Douville · D. Salas-Mélia · S. Tyteca

On the tropical origin of uncertainties in the global land precipitation response to global warming

Abstract Understanding the response of the global hydrological cycle to recent and future anthropogenic emissions of greenhouse gases and aerosols is a major challenge for the climate modelling community. Recent climate scenarios produced for the fourth assessment report of the Intergovernmental Panel on Climate Change are analysed here to explore the geographical origin of, and the possible reasons for, uncertainties in the hydrological model response to global warming. Using the twentieth century simulations and the SRES-A2 scenarios from eight different coupled ocean–atmosphere models, it is shown that the main uncertainties originate from the tropics, where even the sign of the zonal mean precipitation change remains uncertain over land. Given the large interannual fluctuations of tropical precipitation, it is then suggested that the El Niño Southern Ocillation (ENSO) variability can be used as a surrogate of climate change to better constrain the model reponse. While the simulated sensitivity of global land precipitation to global mean surface temperature indeed shows a remarkable similarity between the interannual and climate change timescales respectively, the model ability to capture the ENSO-precipitation relationship is not a major constraint on the global hydrological projections. Only the model that exhibits the highest precipitation sensitivity clearly appears as an outlier. Besides deficiencies in the simulation of the ENSO-tropical rainfall teleconnections, the study indicates that uncertainties in the twenty-first century evolution of these teleconnections represent an important contribution to the model spread, thus emphasizing the need for improving the simulation of the tropical Pacific variability to provide more reliable scenarios of the global hydrological cycle. It also suggests that validating the mean present-day climate is not sufficient to assess the reliability of climate projections, and that interannual variability is another suitable and possibly more useful candidate for constraining the model response. Finally, it is shown that uncertainties in precipitation change are, like precipitation itself, very unevenly distributed over the globe, the most vulnerable countries sometimes being those where the anticipated precipitation changes are the most uncertain.

H. Douville (✉) · D. Salas-Mélia · S. Tyteca
Météo-France/CNRM, 42 avenue Coriolis,
31057 Toulouse Cedex 01, France
E-mail: herve.douville@meteo.fr

1 Introduction

In its Third Assessment Report, the Intergovernmental Panel on Climate Change (IPCC) concluded that both globally averaged surface temperature and precipitation should increase in the twenty-first century (IPCC 2001). However, the model intercomparison revealed that the relationship between the intensity of the global hydrological cycle and global warming is not very robust. At the regional scale, large uncertainties in the precipitation response to increasing amounts of greenhouse gases (GHG) have been reported by many studies (see for instance Douville et al. 2000 or Douville 2005). A global increase in precipitation does not mean that all regions will experience similar changes. Mass continuity suggests for example that enhanced tropical convection will lead to enhanced descending motion, and therefore drying, in the subtropics. Moreover, several studies indicate that the anticipated global increase in precipitation is not associated with an acceleration of the water cycle (Douville et al. 2002; Bosilovich et al. 2005). Global warming also leads to a systematic increase in total precipitable water, so that the average residence time of water in the atmosphere can increase, indicating a possible reduction in the global cycling rate.

Given these uncertainties in the projected global water cycle, placing quantitative constraints on the climate model sensitivity is a major challenge (Allen and Ingram 2002). Unfortunately, the instrumental record is

not very helpful for both statistical and physical reasons. First, the strong spatio-temporal variability of precipitation on a wide range of scales is a major obstacle for detecting trends in precipitation timeseries that show a much weaker signal to noise ratio than temperature records. The situation is particularly critical over the oceanic regions given the lack of direct measurements of precipitation. Satellite estimates do exist, but the length of the record is still too short to be useful for trend analysis. Global atmospheric reanalyses are also available, but are not sufficiently reliable and homogeneous (changes in the nature and number of assimilated data) for this purpose. Global land precipitation (GLP) climatologies are available over the whole twentieth century, and suggest contrasted trends between different regions. In particular, observed precipitation estimates over tropical land areas exhibit a clear reduction after 1976 (Kumar et al. 2004). The second major reason for the difficulty to detect a global increase in precipitation over recent decades is a physical one. In the absence of any significant change in sea surface temperature (SST), increasing the GHG concentrations reduce the intensity of the water cycle (Yang et al. 2003). This effect can be understood as a fast atmospheric response, in contrast with the slower SST response, to a reduction of radiative cooling through a decrease in condensational heating and therefore in precipitation. Therefore, while both the direct radiative heating of enhanced CO_2 and the resulting increase in SST contribute to warm the troposphere, they act against each other in changing global precipitation.

In the present study, we compare the global response of precipitation in a multi-model ensemble of climate scenarios recently achieved for the Fourth Assessment Report of the IPCC. Eight state-of-the-art coupled ocean–atmosphere models have been selected, whose results are consistent with former conclusions about the large uncertainties in the global precipitation response to global warming (IPCC 2001). The focus is on land precipitation for three reasons: the difficulty in accurately measuring precipitation over the oceanic regions, the fact that land precipitation is mainly responsible for the model spread in the response of the global hydrological cycle, and the fact that land precipitation is a major

constraint on future fresh water resources. The main objective is to show that interannual variability, while not a perfect surrogate of climate change, is however useful for understanding the contrasted relationships between GLP (GLP is defined as the area-weighted average of total precipitation over all land grid cells except Antarctica) and surface temperature among different models. The results suggest that deficiencies in simulating teleconnections between tropical rainfall and the equatorial Pacific SSTs, as well as possible changes in these teleconnections, might be partly responsible for the spread in the projected sensitivity of the global hydrological cycle to increasing amounts of GHG.

2 Models and data

Table 1 summarizes the main features of the coupled ocean–atmosphere GCMs used in the present study. Only a subset of eight models has been explored among the 21 models currently available in the IPCC4 data base (http://www-pcmdi.llnl.gov/ipcc/about_ipcc.php). The main reason for this selection is to limit the size of the study. Some models have been however discarded due to the lack of available outputs at the beginning of the study, as well as to major biases (trends) in their present-day (preindustrial) precipitation climatology. The selected subset includes some of the most widely used GCMs and is hopefully representative of the whole IPCC4 data base. It shows a diversity of GLP response that is sufficient to address the issue of the geographical and physical origin of such uncertainties. Horizontal resolution varies typically between 1.4 and 3°. Besides anthropogenic forcings, some experiments also consider the variability of solar and volcanic activity over the twentieth century. All models include sulfate aerosols (only two models also include black and organic carbons), but only a few models consider the semi-direct and/or the indirect effects of these anthropogenic aerosols in their physical package. Though aerosols and their parametrization represent a potential source of uncertainty for simulating the evolution of the global hydrological cycle (Hulme et al. 1998; Liepert et al. 2004), a much larger sample of experiments would be necessary

Table 1 Summary of the features of the selected coupled models, including horizontal and vertical configurations, equilibrium sensitivity to CO_2 doubling, types of anthropogenic aerosols, parametrizations of aerosol effects, as well as the other forcings used in the twentieth century simulations

Brief name	Full name	Atmospheric configuration	ΔT K/(W/m^2)	Anthrop. aerosols	Aerosol effects	Other forcings
CCCMA	cccma_cgcm3	T47 L31	unknown	SU	D	
CNRM	Cnrm_cm3	T42 L45	unknown	SU	D	
CSIRO	Csiro_mk3_0	T63 L18	0.88	SU	D	
GFDL	Gfdl_cm2_0	2.5/2° L24	0.80	SU,B&OC	D	V,S,LU
MPI	mpi_echam5	T63 L31	0.84	SU	D,I1	
MRI	mri_cgcm2	T42 L30	0.86	SU	D	S
NCAR	Ncar_ccsm3_0	T85 L26	0.77	SU,B&OC	D,SD	V
UKMO	ukmo_hadcm3	3.75/2.5° L19	0.87	SU	D,I1	

SU sulfates, *B&OC* black and organic carbons, *D* direct, *SD* semi-direct, *I1* first indirect, *V* volcanoes, *S* solar, *LU* land-use

to tackle this problem and the present study focuses on another potential source of model divergence related to the simulation of internal rather than externally forced variability.

For the sake of simplicity, only the SRES-A2 family of climate scenarios has been analysed. It describes a world of high population growth with more concern for strengthening regional cultural identities, and less concern for rapid economic development. It is based on relatively extreme assumptions about the future GHG emissions that might even exceed the maximum level compatible with the best estimates of available fossil energies (Jancovici 2004). Nevertheless, this choice enables us to maximize the response of the hydrological cycle and therefore to avoid the tedious question of statistical significance. Moreover, it has been verified with the CNRM model that the alternative IPCC4 emission scenarios (SRES-B1 and A1B) lead to a weaker but consistent response of global precipitation.

For each model, the twenty-first century simulation has been concatenated to the twentieth century experiment before analysing the whole timeseries. Annual mean anomalies have been computed relative to the 1971–2000 model climatology. Interannual variability has been isolated from long-term climate change by substracting a simple low-order polynomial fit applied onto the annual mean timeseries. More sophisticated filters do exist, but low-order polynomial fittings are relatively robust, do not require to specify a particular cut-off frequency, and are justified by the shape of the GHG concentration evolution prescribed in the SRES-A2 scenarios. In some cases, parallel integrations using the same radiative forcing have been analysed to assess the robustness of the model response.

As far as monthly observations are concerned, the HadSST.1 climatology (Rayner et al. 2003) has been used to validate the SST simulated in the historical (twentieth century) IPCC simulations. Observed surface air temperature and precipitation over land have been derived from the CRU TS 2.1 climatology (CRU2 hereafter, available at http://www.cru.uea.ac.uk/cru/data) available at a 0.5° horizontal resolution. While this dataset is probably one of the best available to validate the mean land surface climate over recent decades, it has well-known limitations for timeseries analysis. Nevertheless, this problem is alleviated when quasi-global domains are considered like in the present study. Moreover, more homogeneous datasets have also been explored: the CRUT2v surface air temperature climatology (Jones and Moberg 2003) that includes variance adjustment due to changing station density over the 1870–2004 period, as well as the Hulme et al. (1998) precipitation climatology that has also been subject to homogeneity procedures but contains too many missing data to derive global trends in precipitation. Finally, precipitation estimates over the oceanic regions and over the entire globe have been computed from the GPCP version 2 climatology (Adler et al. 2003), which combines in situ and satellite measurements. While model outputs are used at their original resolution, observed climatologies have been interpolated onto a common 128×64 horizontal grid before analysis.

3 Global precipitation response in the SRES-A2 scenarios

Figure 1 shows the zonal mean present-day (1971–2000) precipitation climatologies in the eight coupled GCMs, as well as the corresponding changes between 2071–2100 and 1971–2000. Generally speaking, all models show a reasonable climatology at the end of the twentieth century compared to the GPCP and CRU2 (land only) observations. The main discrepancies shared by most models is an overestimation of land precipitation in the southern mid-latitudes, and of oceanic rainfall in the tropics (the well-known "double-ITCZ" error). Looking at climate change in the SRES-A2 scenarios, all models show an increase in the extratropical precipitation over both land and sea. In the tropics, the situation is much more contrasted. While most models indicate enhanced oceanic rainfall around the equator and a corresponding drying in the subtropics (enhanced Hadley circulation), the precipitation anomalies over tropical land are very uncertain.

This result is confirmed by Fig. 2 that illustrates the transient response of the annual mean 2-m temperature and precipitation anomalies relative to the 1971–2000 model climatologies. While most models show a remarkable agreement in the projected global warming over the twenty-first century, the range in the global precipitation response is larger, especially over land, and is mainly related to contrasted rainfall anomalies in the tropics. In this particular area, three models (CSIRO, GFDL and UKMO, CGU hereafter) show a decrease in annual mean rainfall over land, in keeping with their low estimates of the global mean precipitation increase, while the other models show a weak, medium or strong increase. This huge uncertainty in the tropical land precipitation anomalies is not associated with a similar spread in the temperature anomalies, that are relatively consistent with the global estimates, though not surprisingly stronger because of the land amplification of the ocean warming. Note finally that the CRU2 precipitation timeseries (thick black lines in Fig. 2) confirm that the tropics exert a major influence on the GLP evolution, but show a stronger multi-decadal variability than in most coupled GCMs, with an abrupt shift in the mid-1970s that is consistent with Kumar et al. (2004).

Figure 3 looks at the relationship between the simulated global warming and the GLP anomalies at the annual time scale. All anomalies are again estimated against the 1971–2000 model climatologies. A quadratic regression is estimated for all models as well as for the CRU2 climatology. In keeping with the tropical response described in Fig. 2, the CGU models show a weak sensitivity of the global land hydrological cycle to global warming, since the increase in extratropical
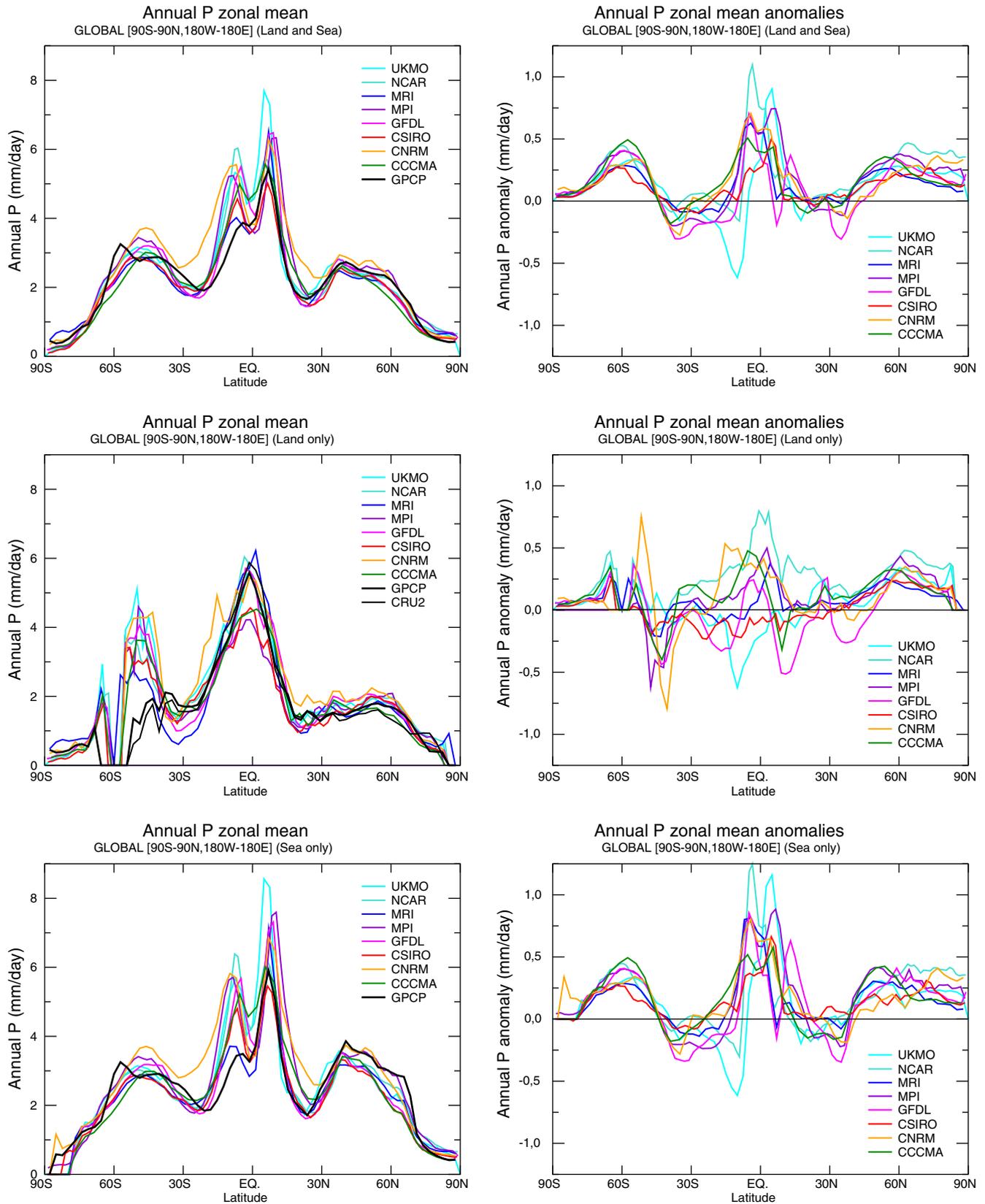
Fig. 1 Zonal and annual mean present-day (1971–2000) precipitation climatology in models and observations (*left panels*), as well as zonal and annual mean precipitation anomalies (2071–2100 – 1971–2000) in the SRES-A2 climate scenarios (*right panels*). The results are shown for both land and sea (*top panels*), land only (*middle panels*) and ocean only (*lower panels*)
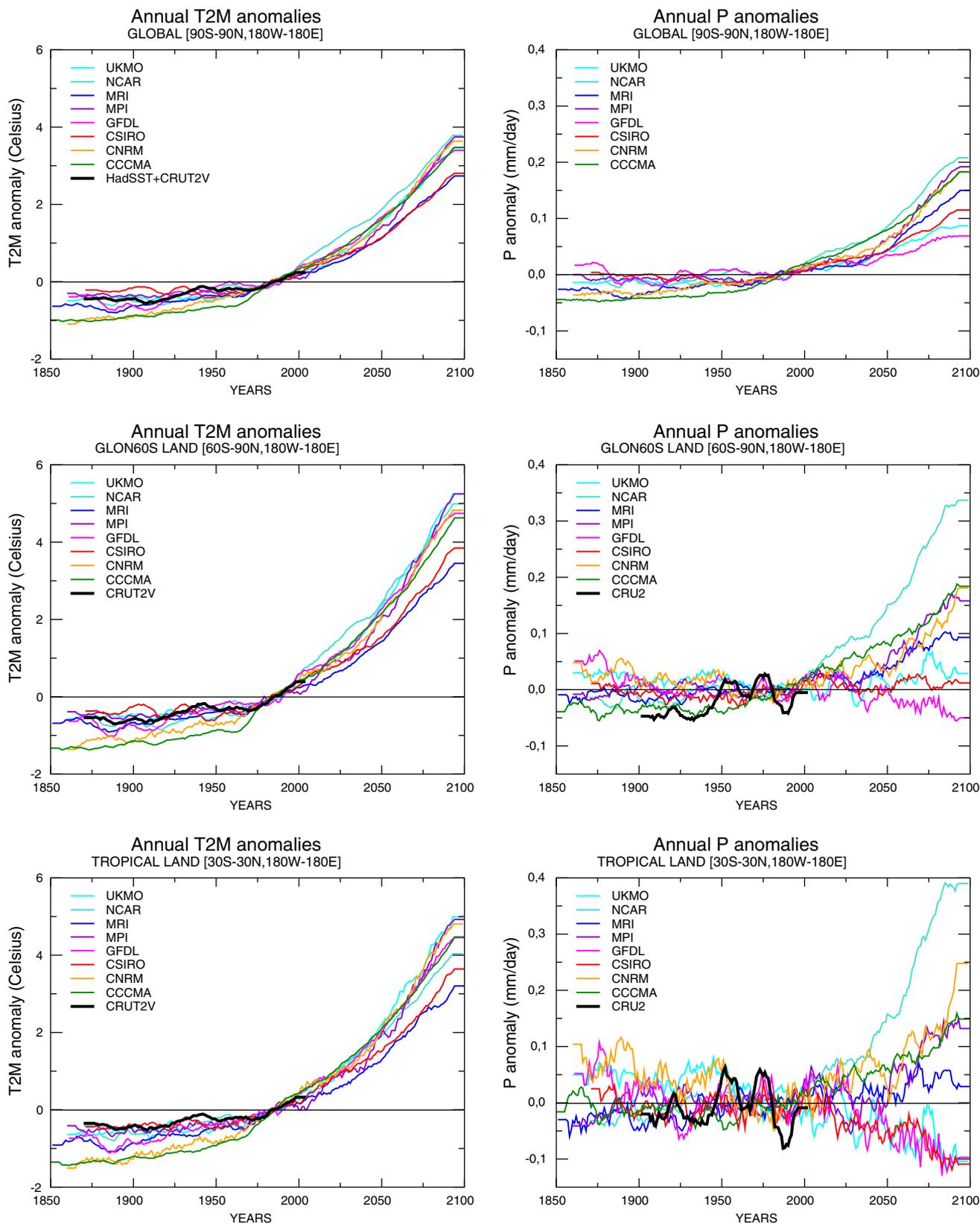
Fig. 2 Transient 11-year moving average response of annual mean surface air temperature (*left panels*) and annual mean precipitation (*right panels*) to anthropogenic radiative forcing relative to the 1971–2000 model climatologies. The results are shown for global means (*top panels*), global means over land (*middle panels*) and tropical means over land (*lower panels*). Note that global land averages always exclude Antarctica where precipitation measurements are scarce and of poor quality
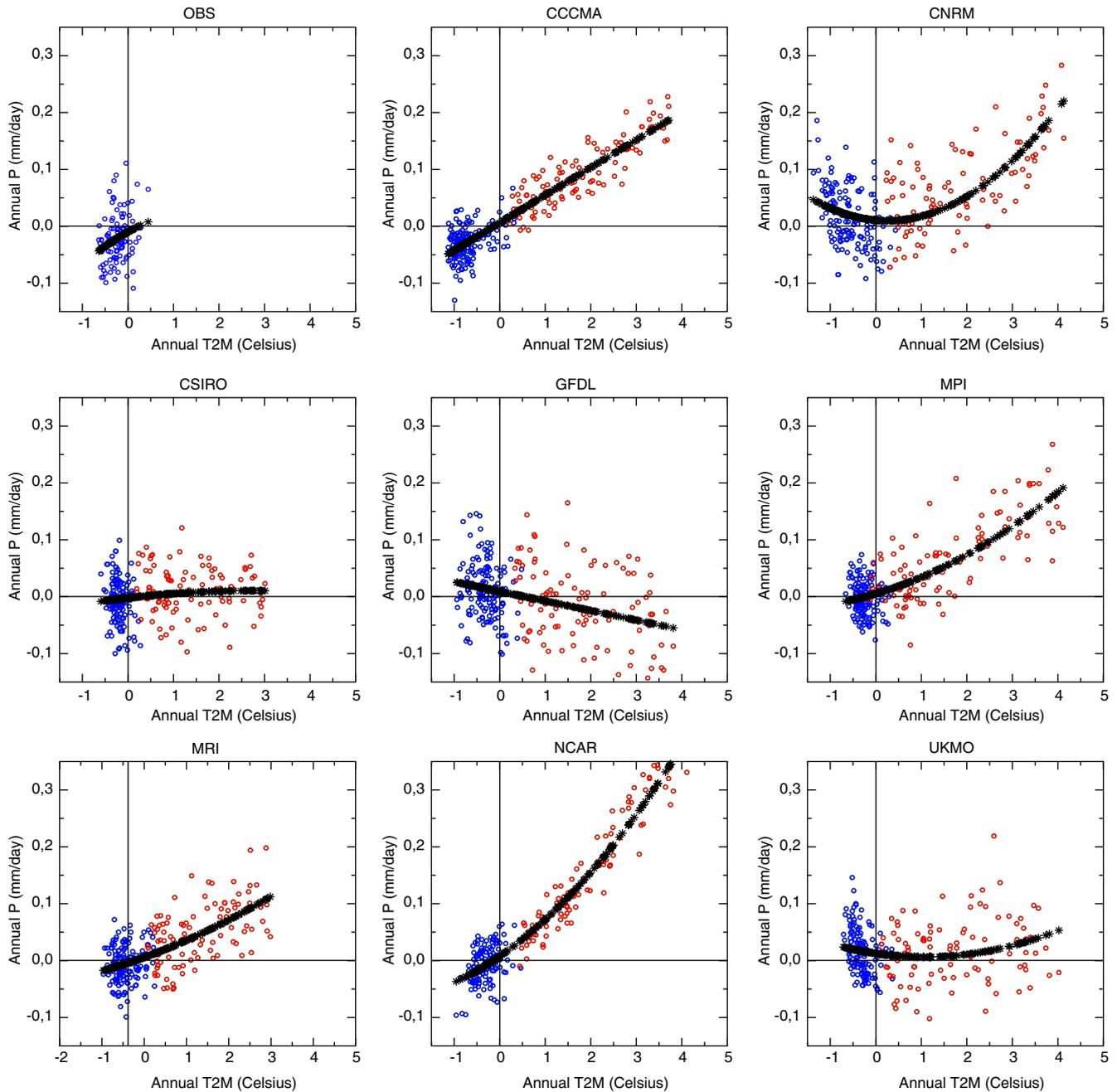
Fig. 3 Scatterplots of annual mean global land precipitation (*GLP*) anomalies versus annual mean global 2-m temperature anomalies in the observations (here CRU2 for precipitation and HadSST.1 combined with CRUT2v for temperature) and in the coupled simulations. Blue symbols denote years before 2000, while *red* symbols are used for the twenty-first century scenarios. *Black* symbols represent a quadratic fit of the scatterplots

precipitation (Fig. 1) is more or less counterbalanced by a decrease in tropical rainfall. In contrast, the NCAR model shows a very strong sensitivity, which is also consistent with the results in Figs. 1 and 2. The CRU2 timeseries suggests an intermediate response, but is too short and not sufficiently reliable to constrain the model response. Another striking result is the lack of GLP variability in the NCAR and CCCMA models, a feature that will be explained in Sect. 5.

In summary, the IPCC4 projections of GLP remain very uncertain even in the most extreme SRES-A2 scenarios. These uncertainties originate mainly from the tropics where even the sign of the rainfall anomalies is uncertain. This is particularly critical given the relatively high vulnerability of the tropical regions as far as water resources are concerned. Understanding the reasons for such uncertainties is therefore a major challenge and will be the focus of the continuation of the present study.

4 Interannual variability as a surrogate of climate change?

While the detection of changes in the global hydrological cycle remains a difficult task given the strong interannual variability of precipitation, this variability can be used to evaluate the possible relationship between GLP and global mean surface temperature in the instrumental record (twentieth century) and in the coupled simula-tions (from the second half of the ninetieth century to 2100). For this purpose, it is first necessary to detrend both temperature and precipitation timeseries. This is done simply through the use of a polynomial fit, linear for the relatively short instrumental record, at third order for the simulations.

Figure 4 shows the resulting scatterplots, using the same colour convention as in Fig. 3 (blue before 2000 and red after), but based on detrended rather than raw annual anomalies. For each model, three linear
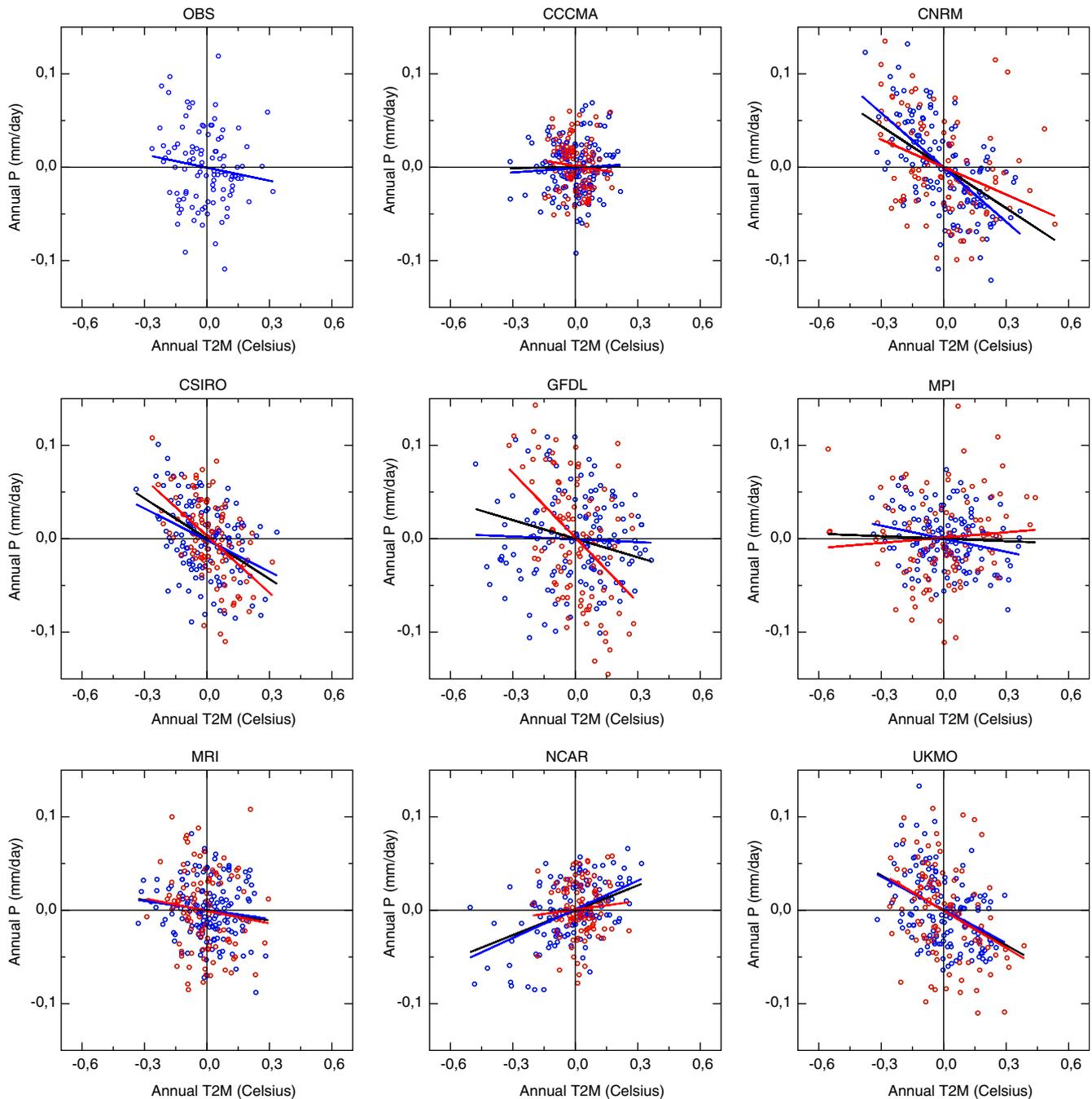

Fig. 4 Same as Fig. 3, but using detrended precipitation and temperature timeseries using a linear (observations) or a third order polynomial fit (simulations). Three linear fits are shown for the whole distribution (*black line*), the years before 2000 (*blue lines*), and the twenty-first century scenarios (*red lines*)

regressions have been calculated for the whole timeseries (in black) as well as for the two sub-periods (in blue and red). The regression coefficients and the fractions of explained variance are summarized in Table 2. While the observations do not show any significant linear relationship between GLP and global mean temperature, the models show a large variety of behaviours, the fraction of explained variance varying between 0 and 39% over the twentieth century. Interestingly, the CGU models exhibit a relatively strong and robust decrease in GLP with increasing temperature, while the NCAR model, in contrast, shows a robust positive relationship. These contrasted sensitivities at the interannual timescale are remarkably consistent with the climate change responses described in Fig. 3. The main exception is the CNRM model that shows a relatively strong precipitation sensitivity to global warming (Fig. 3), but a negative correlation at the interannual timescale (Fig. 4). Note however that this model shows a non-linear precipitation response to global warming, which is partly related to a weakening of the GLP-temperature relationship during the twenty-first century. Conversely, the GFDL model shows a strenghtening of the GLP–temperature relationship, which is also consistent with its low sensitivity to global warming.

Still based on the detrended timeseries, Fig. 5 compares the spatial distribution of the 1951–2000 correlations between the annual mean GLP and the annual mean grid-point surface temperature (land and sea) simulated by each model. Also shown are the corresponding observed correlations between the CRU2 GLP and the HadSST.1 detrended anomalies. The instrumental record shows a dominant influence of the tropical Pacific SSTs on the GLP interannual variability, which is more or less reproduced by six of the eight models. These correlation patterns are generally symmetric to the SST correlations calculated with the Niño-3 SST index (Fig. 6) and are therefore dominated by the well-known El Niño Southern Oscillation (ENSO), which has indeed a major influence on the tropical

hydrological cycle (Soden 2000). Cold anomalies in the eastern and/or central tropical Pacific (La Niña events) are generally associated with stronger GLP, in keeping with the well-known ENSO teleconnections with the Asian and African monsoons (Diaz et al. 2001; Brooks 2004). Two models (CCCMA and NCAR) fail to capture the observed correlation pattern in Fig. 5, though they do show reasonable spatial correlations with the Niño-3 SSTs (especially CCCMA). Interestingly, these are the only models that exhibit a positive temporal correlation between GLP and global mean surface temperature at the interannual timescale during the twentieth century (Table 2 and Fig. 4). Their relatively strong hydrological sensitivity to global warming (as well as their low interannual variability of GLP) might be therefore related to some difficulties in simulating realistic ENSO-precipitation teleconnections.

5 Influence of ENSO variability

Results presented in Sect. 4 suggest a possible link between the GLP sensitivity to global mean surface temperature at the interannual and climate change timescales respectively, as though the anthropogenic signature in the global hydrological cycle found in the IPCC4 simulations was strongly dependent on the nature of the ENSO-precipitation teleconnections in each model. The major influence of ENSO on the GLP interannual variability is confirmed by Table 2, which gives the regression slopes and the fractions of explained variance for both models and observations. Unlike global mean surface temperature, the Niño-3 SSTs show a significant anti-correlation with GLP in the observational record. In keeping with the results in Fig. 5, all models except CCCMA and NCAR are able to simulate this relationship.

In order to understand the role of the ENSO–GLP teleconnection, it is important to analyse both the realism and the possible evolution of the ENSO variability

Table 2 Regression coefficient (slope) of GLP on global mean surface air temperature and on Niño-3 SSTs

Dataset	Regression on global mean T2m		Regression on Niño-3 SST	
	Twentieth century	Twenty-first century	Twentieth century	Twenty-first century
CRU2-HCT2v	−0.05 (2)		**−0.04 (28)**	
Hulme-HCT2v	−0.11 (4)		**−0.07 (25)**	
CCCMA	0.02 (0)	−0.04 (1)	0.01 (0)	−0.01(1)
CNRM	**−0.19 (39)**	**−0.10 (12)**	**−0.02 (36)**	**−0.01 (9)**
CSIRO	**−0.11 (14)**	**−0.20 (27)**	**−0.04 (42)**	**−0.04 (36)**
GFDL	−0.01 (2)	**−0.23 (20)**	**−0.03 (18)**	**−0.06 (45)**
MPI	**−0.05 (6)**	0.02 (1)	**−0.01 (17)**	−0.01 (2)
MRI	−0.03 (2)	−0.04 (2)	**−0.03 (16)**	**−0.03 (24)**
NCAR	**0.10 (24)**	0.03 (1)	−0.00 (0)	−0.01 (5)
UKMO	**−0.12 (17)**	**−0.13 (12)**	**−0.03 (27)**	**−0.03 (20)**

The percentage of total variance that is explained by the regression is indicated in brackets. Slopes that are significant at the 1% level are in bold. All regresssions are based on detrended annual mean anomalies and are estimated for the twentieth and twenty-first century separately
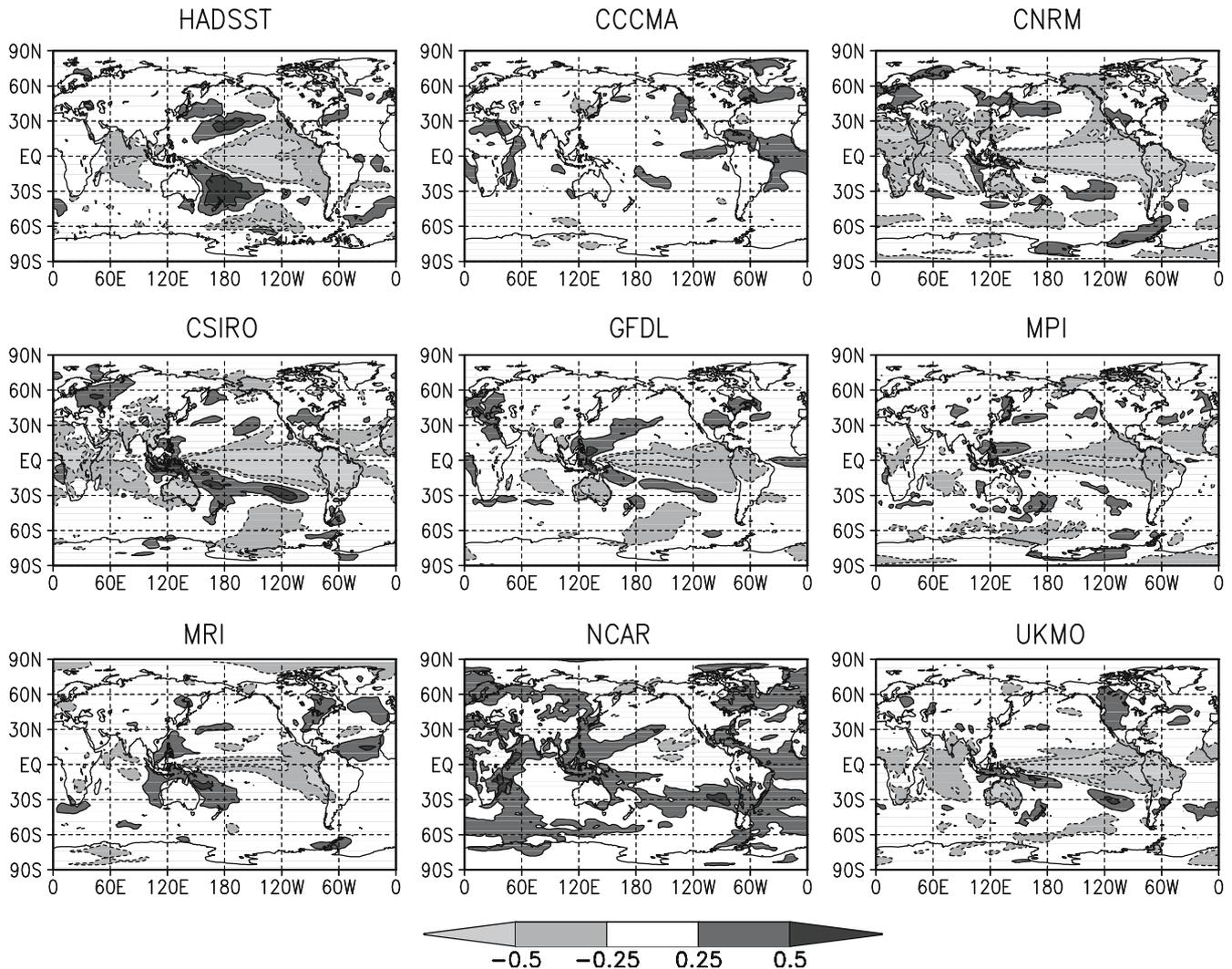
Fig. 5 Time correlations between annual mean local surface temperature anomalies and annual mean GLP anomalies over the 1951–2000 period. Model correlations are shown over both land and sea, while the observed correlations are based on the CRU2 GLP and the HadSST.1 climatology. All anomalies are detrended

in the IPCC simulations (Fig. 7). Most models capture the present-day annual cycle of the ENSO variability with a maximum activity during the boreal winter season. Some models (CCCMA and MRI) clearly underestimate the ENSO signal, while others (CNRM and, to a lesser extent, MPI) show an opposite behaviour. These systematic biases are relatively stable at both monthly and multi-decadal timescales. Nevertheless, various models show a significant multi-decadal modulation of the ENSO variability. Several models indicate a possible increase in the variability of the Niño-3 SSTs during the twenty-first century. This is for example a robust response of the MPI coupled model, that shows a similar behaviour in two replications of the SRES-A2 scenario (not shown) as well as in former IPCC scenarios (Timmerman et al. 1999). Such a response is consistent with the positive trend found in the HadSST.1 climatology over the twentieth century, which however must

be considered very carefully given the heterogeneous and short instrumental record.

Nevertheless, the response of the ENSO variability to global warming is not the focus of the present study. Fig. 7 helps understand why some models poorly capture the ENSO–GLP relationship (possible influence of the underestimated ENSO variability in the CCCMA model) and how possible changes in the ENSO activity can affect the response of the global hydrological cycle in the SRES-A2 scenarios. With regards to this last issue, Fig. 8 shows lead/lag correlations between annual mean GLP (averaged between months 1 and 12) and monthly Niño-3 SSTs in a 36-month window starting 1 year before and ending 1 year after the GLP averaging period. For each model, the simulated correlations for present-day climate (1951–2000) are superimposed onto the observed correlations over the same period, as well as onto the correlations simulated in the second half of the
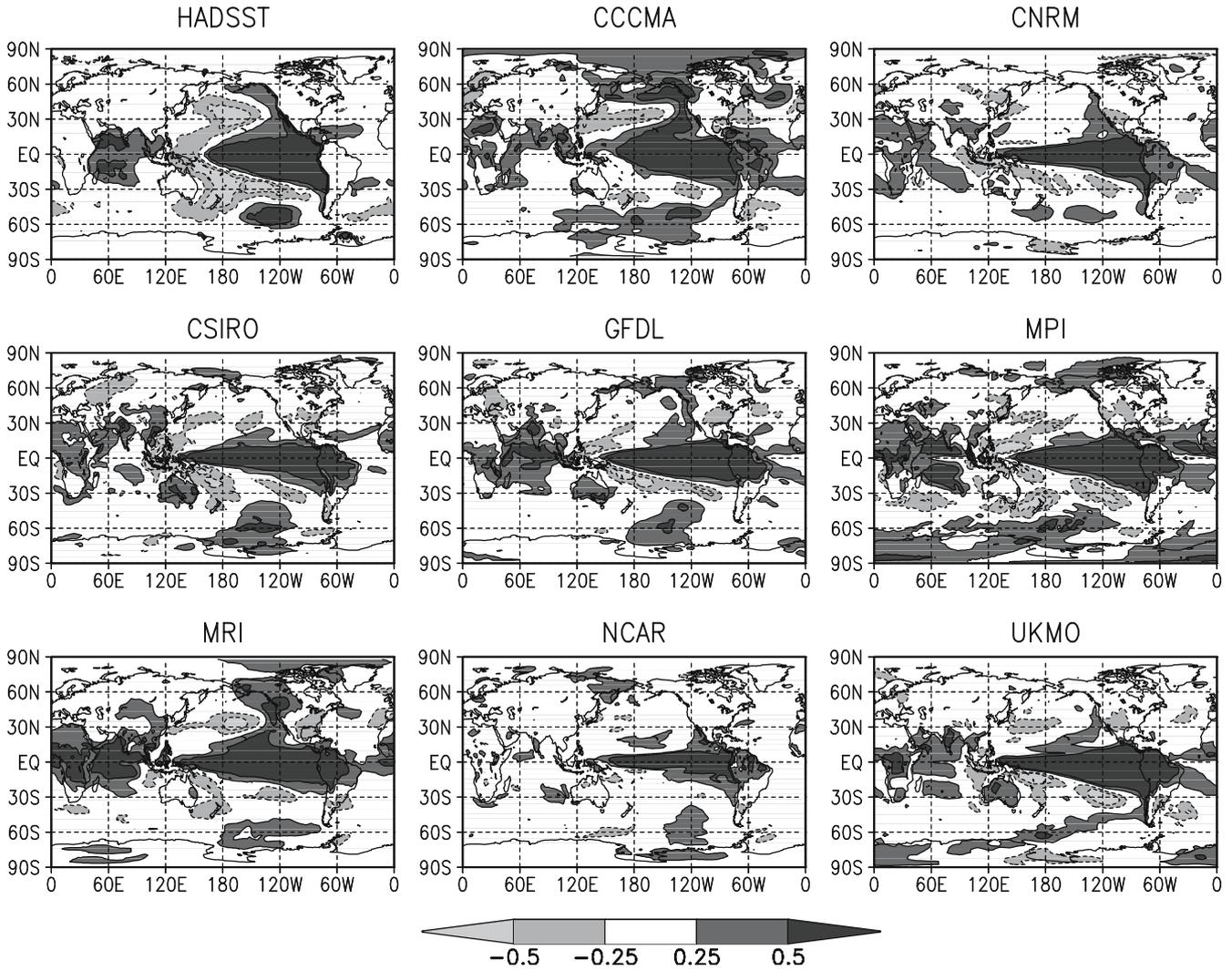
Fig. 6 Time correlations between annual mean local surface temperature anomalies and annual mean Niño-3 SST anomalie over the 1951–2000 period. Model correlations are shown over both land and sea, while the observed correlations are based on the HadSST.1 climatology. All anomalies are detrended
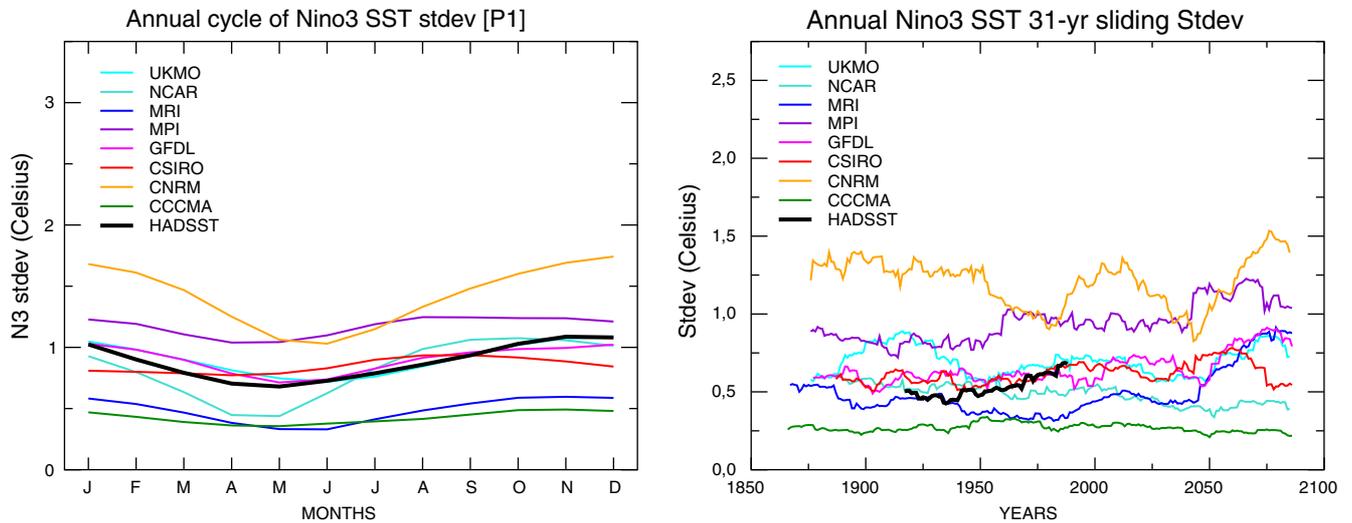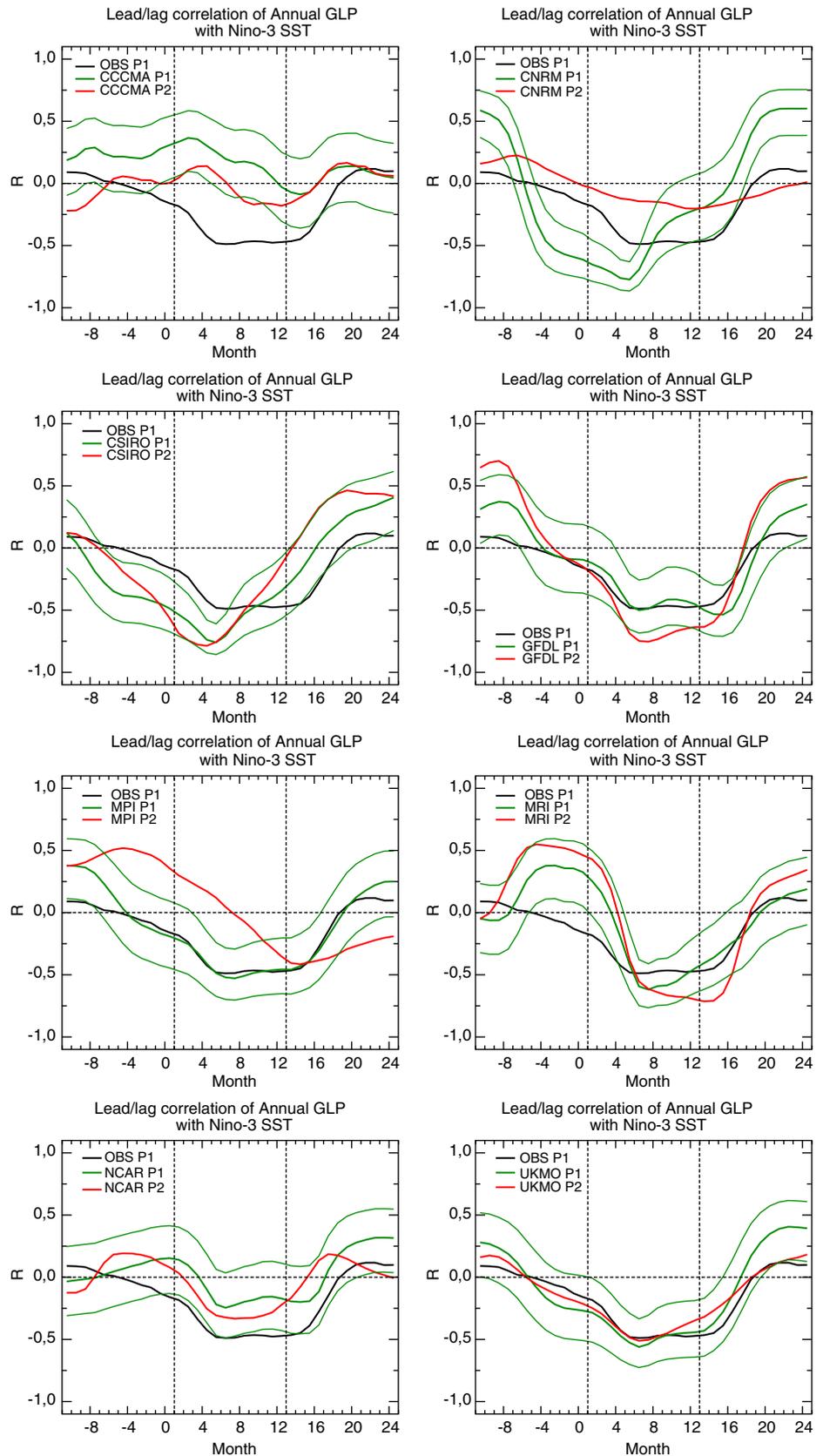

Fig. 7 Mean annual cycle of Niño-3 SST standard deviations for present-day conditions (1971–2000, *left panel*), and 31-year moving averages of the standard deviation of annual mean detrended Niño-3 SST anomalies (*left panels*) in both the HadSST.1 climatology and the simulations

Fig. 8 Lead-lag monthly correlations between annual mean GLP (averaged between months 1 and 12) and monthly Niño-3 SSTs over a 3-year period starting at month-11 and ending at month 24. For each model, the simulated correlations for present-day climate (P1:1951–2000, in green) are superimposed onto the observed correlations over the same period (in *black*), as well as onto the correlations simulated in the second half of the twenty-first century (P2:2051–2100, in *red*). Also shown is the 95% confidence interval of the simulated present-day correlations (thin *green lines*). All correlations are based on detrended timeseries

twenty-first century. Also shown is the 95% confidence interval of the simulated present-day correlations. While some models capture the seasonal evolution and the magnitude of the correlations, two models (CCCMA and, though to lesser extent, NCAR) underestimate the maximum anti-correlation that is observed from month

4 to month 15, and two models (CNRM and CSIRO) anticipate and overestimate this maximum. Most models do not show significant changes in the correlations at the end of the twenty-first century. Nevertheless, GFDL seems to reinforce the anti-correlation, while, in contrast, CNRM and MPI show a strong weakening of the ENSO-GLP relationship.

This result is confirmed by Fig. 9 showing running correlations between GLP and Niño-3 SSTs annual mean detrended anomalies. Two estimates are provided

for the observed correlations. For some models, three replications of the historical and SRES-A2 scenario experiments have been used to assess the robustness of the multi-decadal variability of the correlations. This precaution is very important given the strong natural modulation of running correlations between pairs of stochastic timeseries (Gershunov et al. 2001; Diaz et al. 2001). For the CNRM model, which was integrated only once for each IPCC4 scenario, three additional scenarios (Commit, B1 and A1B) are also shown. They confirm
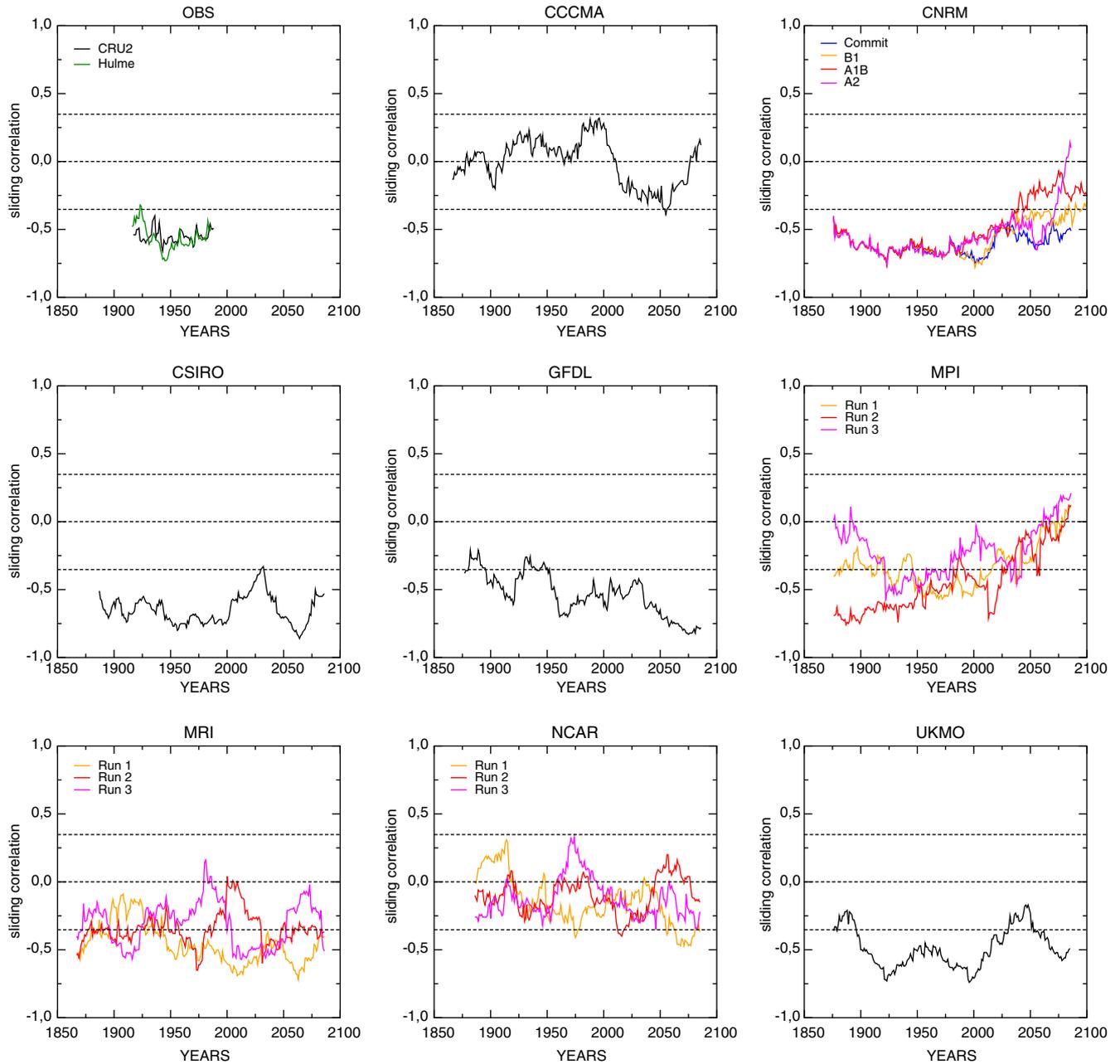

Fig. 9 31-year running correlations between detrended annual mean anomalies of GLP and Niño-3 SSTs. Observed correlations are based on two precipitation datasets (CRU2 and Hulme) and on the Niño-3 index derived from the HadSST.1 climatology.

Simulated correlations are shown for three rather than one replication of the historical and SRES-A2 integrations for the MPI, MRI and NCAR models. The results of other IPCC4 emission scenarios are shown for the CNRM model

that, superimposed on natural multi-decadal fluctuations, the CNRM model anticipates a weakening of the ENSO-GLP relationship in the most severe scenarios (SRES-A1B and A2). Note that this weakening is also found in another recent SRES-A2 scenario in which CNRM-CM3 has been coupled with an integrated impact model, while our 500-year preindustrial run does not show such dramatic changes in the correlations (not shown). Note also that no weakening of the ENSO-tropical rainfall teleconnections was found in former SRES-B2 scenarios based on CNRM-CM2 (Ashrit et al. 2003; Camberlin et al. 2004) rather than CNRM-CM3. This result is consistent with the weak modulation of the ENSO-GLP relationship found in the IPCC4 SRES-B1 scenario (Fig. 9).

Besides CNRM, another model shows a substantial weakening of the ENSO teleconnection with GLP, namely the MPI model. In this case, this weakening is also robust since it appears in the three parallel integrations shown in Fig. 9. This common response between CNRM and MPI is consistent with the significant upward change found in the relationship between GLP and global mean surface temperature before and after year 2000 in Fig. 4. Conversely, the opposite downward change found in the GFDL model can be related to a strenghtening of the ENSO–GLP correlations.

6 Looking for a better surrogate of climate change?

Section 4 has suggested a link between the GLP sensitivity to global mean temperature at the interannual and climate change timescales, respectively, thereby providing a possibility to constrain the models' response according to their ability to capture the observed interannual sensitivity. It must be, however, emphasized that interannual variability remains a poor surrogate of climate change. Interannual fluctuations of global mean temperature are dominated by the ENSO variability and are associated with specific patterns of tropical SST anomalies. For global warming, unlike ENSO, the SST change is more uniform, so that changes in the atmospheric large-scale circulation are expected to be smaller and the precipitation response may instead be dominated by radiative and thermodynamic effects (Lau et al. 1996).

To address this major limitation, it might be interesting to repeat the former analysis of the relationship between GLP and global mean temperature by focusing on a subset of years where the interannual SST anomalies resemble the tropical [30°S–30°N] SST patterns of climate change. These patterns and their global extension are shown in Fig. 10 where the annual mean SST change has been plotted in each model after removing the tropical mean SST warming. All models indicate a stronger warming over the equator than over the subtropical oceans (especially those of the southern hemisphere), but there is a large variety of SST patterns in the tropical Pacific with only a subset of models (mainly

CNRM, MRI, CCCMA and UKMO) showing an El Niño-like response. This pattern shows some similarity with the recent evolution found in the HadSST.1 climatology (upper left panel in Fig. 10), which however is mostly dominated by the Pacific Decadal Oscillation (PDO). Note once again that the ENSO response to global warming remains a matter of debate (Diaz et al. 2001) and is beyond the scope of the present study. Also unclear is the nature of the interaction between the tropical and extratropical Pacific (Gershunov et al. 1998; Diaz et al. 2001). Bearing these uncertainties in mind, our purpose is here just to describe the tropical SST patterns of climate change found in the various models, and to look for individual years where the detrended SST anomalies exhibit similar patterns.

For each model and each year, the similarity between the detrended anomalies and the climate change patterns shown in Fig. 10 is measured through a simple anomaly correlation coefficient (ACC) within the tropical belt [30°S–30°N]. Then, it is possible to construct composites based on a minimum threshold for the ACC. Given the range of the maximum ACCs among the different models (typically from 0.35 to 0.55), a threshold of 0.3 has been selected. The resulting composites of annual mean precipitation anomalies are shown in Fig. 11, only for the four models (CNRM, CSIRO, MPI and MRI) where the 0.3 ACC threshold is exceeded for at least 30 years. They can be compared to the annual mean precipitation changes found in the SRES-A2 scenarios (Fig. 12). Though such a comparison remains qualitative, striking similarities appear in the tropics, suggesting that the subsets of selected years indeed represent an improved surrogate of the late twenty-first century tropical climate compared to the whole timeseries.

It is then interesting to repeat the scatterplots shown in Fig. 4, but using different colours for different ACC intervals rather than different centuries. The results are shown in Fig. 13. Again, only those models where interannual variability is potentially a good surrogate of climate change are presented. Given the variable number of years where a given ACC threshold is exceeded among the different models, the timeseries have been divided in five subsets corresponding to the quintiles (i.e. the 20% quantiles) of the ACC distributions. Three linear regressions have been estimated for the whole timeseries (in black), the lower quintile (in blue), and the upper quintile (in red).

Figure 13 is more enlightening than Fig. 4 about the possible reasons for the contrasted GLP sensitivity to global warming among the four models. Comparing the upper quintile with the remainder of the distribution allows us to detect a possible impact of the tropical SST pattern of climate change on GLP (i.e. the tropical circulation impact), but also to isolate a "residual" impact of global warming by comparing the slopes of the red versus black regressions. This residual impact can be attributed to several mechanisms (both dynamical and non-dynamical) and is therefore difficult to interpret.
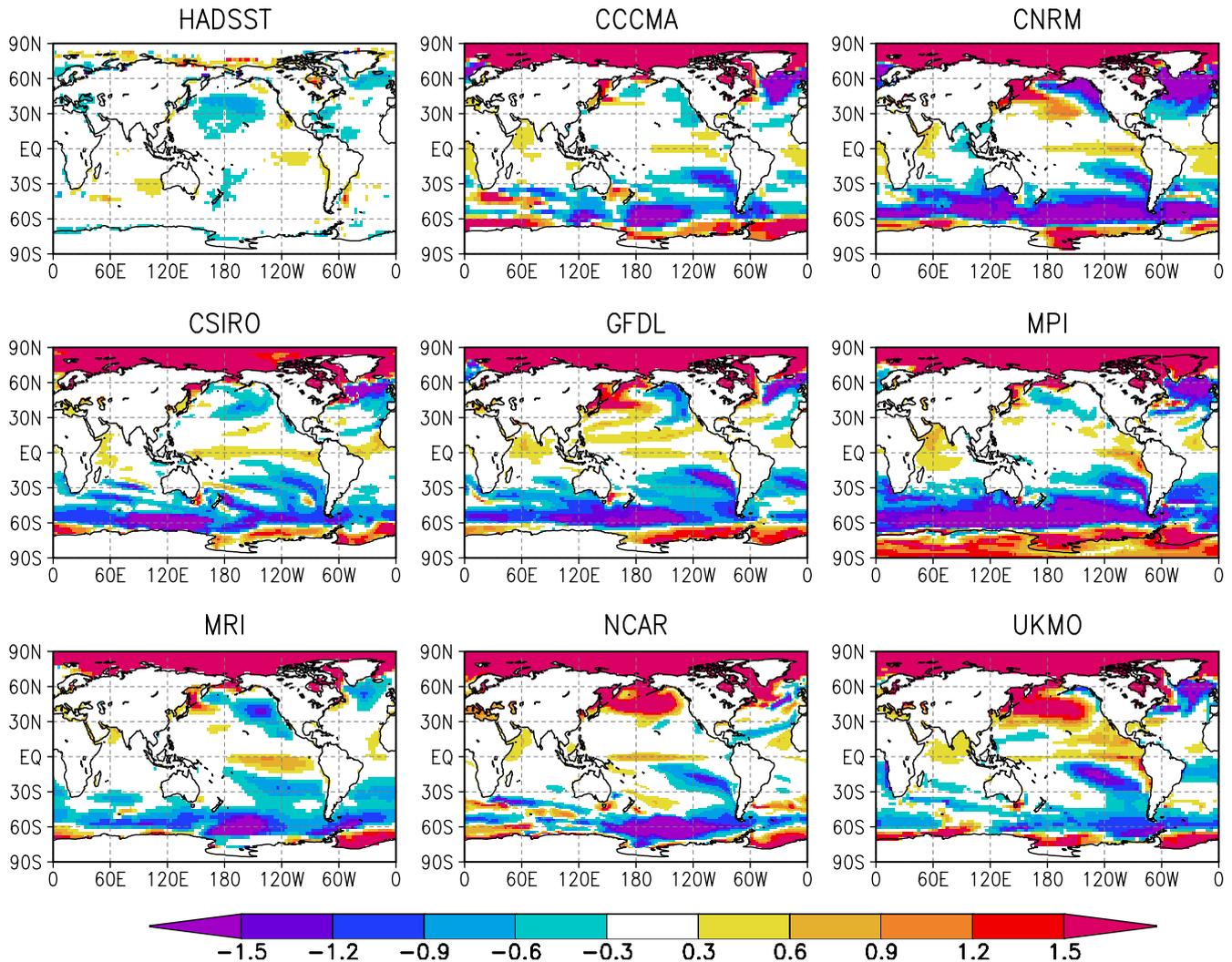
Fig. 10 Patterns of annual mean SST anomalies (K) after removing the spatial mean warming found in the tropics (30°S–30°N). Anomalies are calculated as 2071–2100 − 1971–2000 in the SRES-A2 climate scenarios, and as 1976–2000 − 1951–1975 in the HadSST.1 climatology to provide a crude estimate of the late twentieth century climate change in the instrumental record

The CSIRO model, which is here the only member of the low-sensitivity group (CGU models), shows lower than normal GLP in the upper quintile, indicating that the tropical SST pattern of climate change limits the precipitation increase in this model. Moreover, the upper quintile regression shows a significant anti-correlation between GLP and temperature at the interannual timescale (even stronger than for the whole timeseries), indicating that the residual impact also contributes to moderate the model sensitivity. The other models, which belong to the medium-sensitivity group, exhibit a weaker tropical circulation impact, and show a neutral or positive residual impact (as indicated by the regression slope of the upper quintile).

Note finally that the CNRM model shows very contrasted regressions between the upper quintile (in red) and the remainder of the distribution (in black). This remark confirms that interannual variability is not a perfect surrogate of climate change and that it is possible

to define a better surrogate through the stratification technique proposed in this section. The medium rather than low sensitivity of the CNRM model is now easier to interpret than at the end of Sect. 4. The first reason is the absence of anti-correlation between GLP and global mean surface temperature when looking at a better surrogate of climate change. The second one is related to the weakening of the ENSO-GLP teleconnection found in Sect. 5, which contributes to limit the impact of the ENSO-like SST response in this model.

7 Discussion and conclusion

In keeping with the conclusions of the Third Assessment Report (IPCC 2001), the IPCC4 simulations based on the SRES-A2 scenarios show large uncertainties in the response of the global hydrological cycle to increasing amounts of GHG. The uncertainty is stronger over land
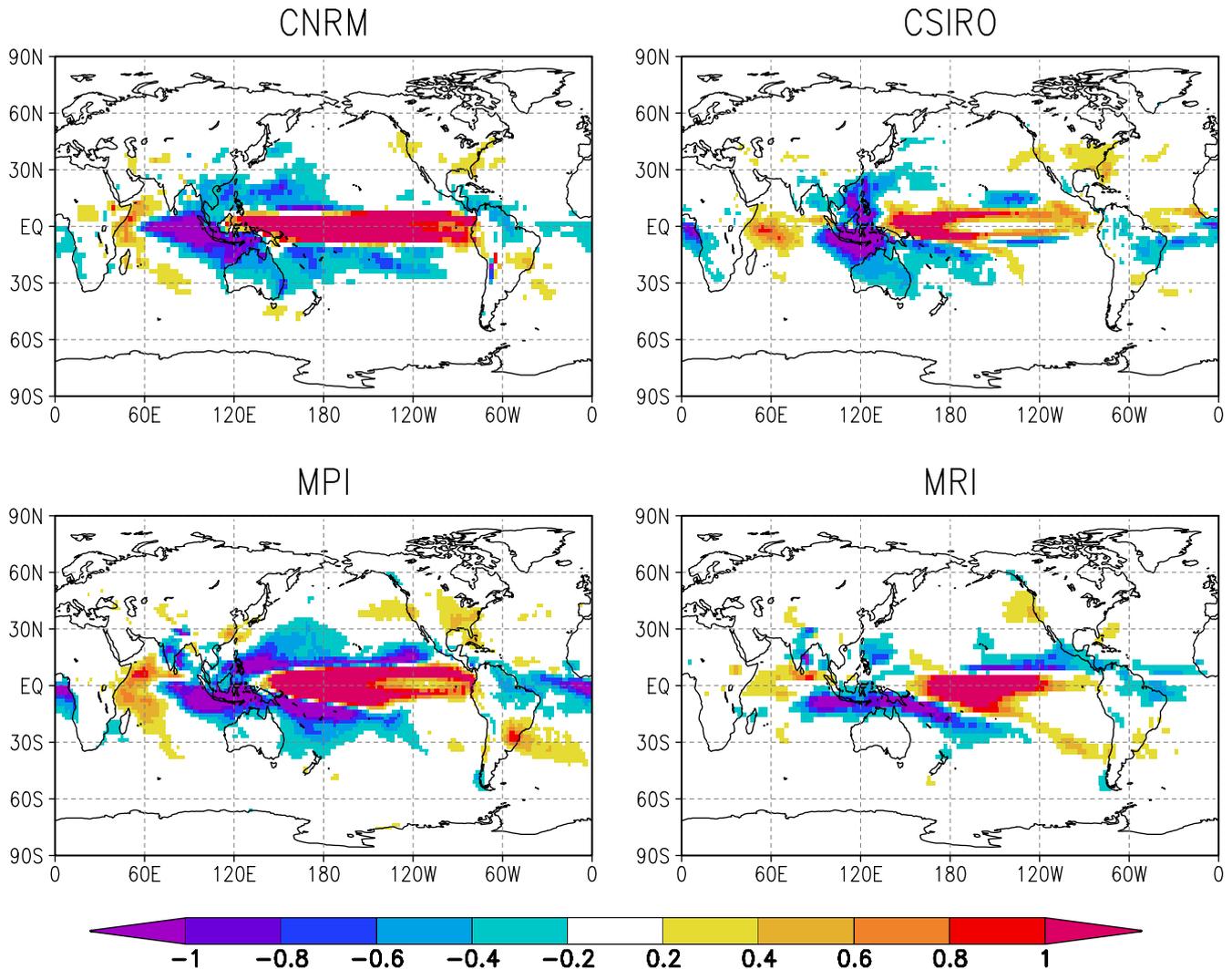
Fig. 11 Composites of annual mean precipitation anomalies (mm/day) for a subset of years when the detrended annual mean tropical SST anomalies resemble (ACC > 0.3) the patterns found in Fig. 10. The results are shown only when a sufficient number of years allows us to built a sufficiently robust composite (four models)

than over oceanic surfaces and mainly originates from tropical land areas. This is a major problem given the increasing demand of water projected over the twenty-first century, especially in the tropics where the population growth should be the strongest. In a world where water might become, like oil, a natural resource that will have to be exchanged between countries in excess and in deficit, it is not only the regional precipitation anomalies but also the GLP response that needs to be better defined in order to anticipate when global freshwater resources might be no longer sufficient to satisfy global demand.

Reducing the uncertainties by constraining the model response is therefore a major challenge (Allen and Ingram 2002). Given the relative success of multi-model ensemble simulations in the field of dynamical seasonal forecasting, it is tempting to use a similar strategy for climate scenarios (Murphy et al. 2004). Note however that seasonal predictions usually show very limited

scores when no significant SST anomalies appear in the tropics, the main source of atmospheric predictability at the global and seasonal to interannual timescales being undoubtedly the ENSO variability. Unlike ENSO, global warming is associated with relatively uniform SST changes in the tropics. This remark suggests that predicting climate change is in some sense more challenging than seasonal forecasting. It is not only the response of the divergent atmospheric circulation (and of the associated teleconnections) to the anticipated tropical SST anomalies that must be captured, but also the direct radiative and thermodynamic impacts of increasing amounts of GHG that determine the 3D structure of the atmospheric warming.

The present study suggests that ENSO variability remains an interesting surrogate of climate change as long as the global tropical response of the hydrological cycle is analysed rather than the more robust extra-tropical response or more regional precipitation
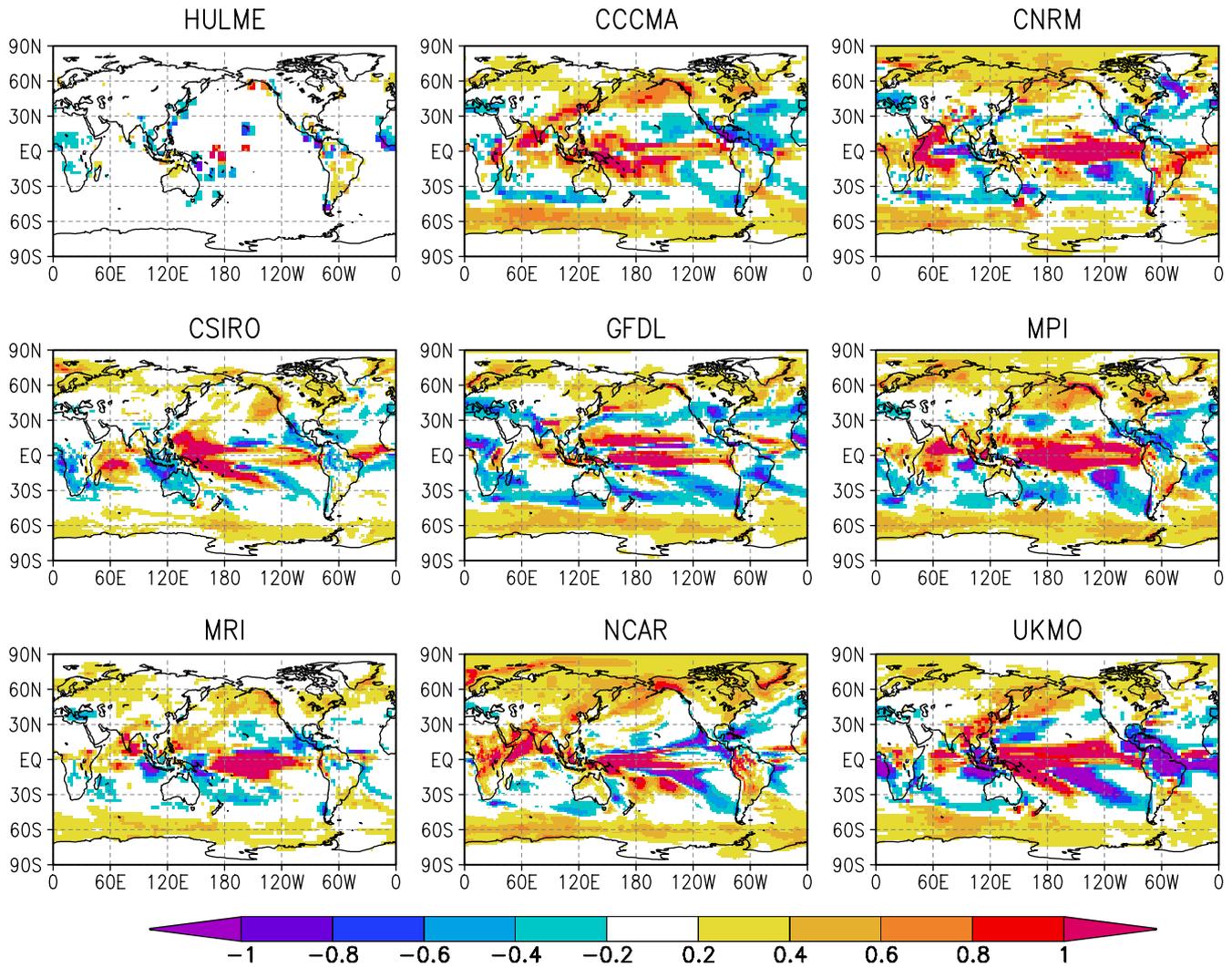
Fig. 12 Patterns of annual mean precipitation anomalies (mm/day). Anomalies are calculated as 2071–2100 − 1971–2000 in the SRES-A2 climate scenarios, and as 1976–2000 − 1951–1975 in the Hulme climatology to provide a crude estimate of the late twentieth century climate change in the instrumental record
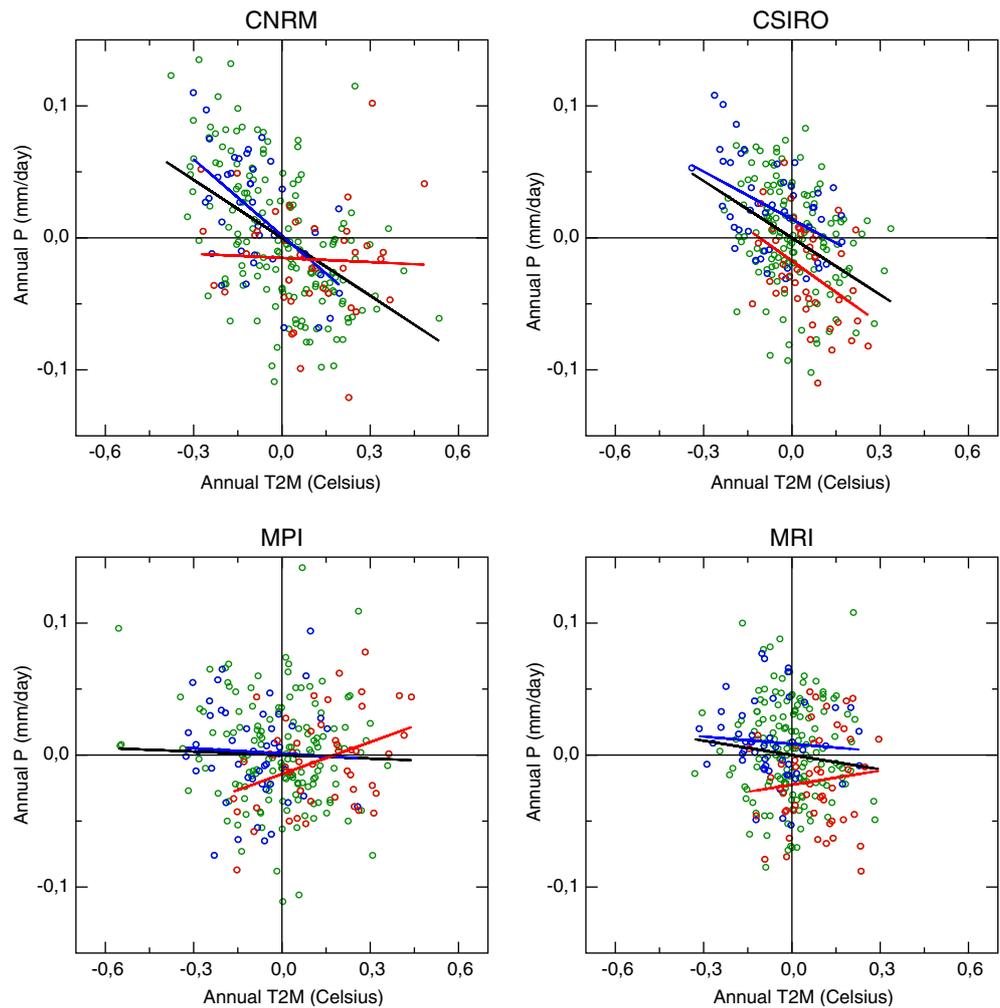
anomalies. This finding is consistent with the results of Lau et al. (1996). The relative consistency of the GLP sensitivity to global mean surface temperature between the interannual and the climate change timescales seems to provide an opportunity to constrain the twenty-first century climate projections. Besides the simulation of the present-day climatology, the simulation of the twentieth century ENSO variability and teleconnections appears to be another suitable and possibly more useful candidate to put the climate scenarios into perspective.

Nevertheless, the authors recognize that ENSO cannot be blamed for all model deficiencies in simulating the interannual variability of precipitation. Other modes of variability, within and outside the tropics, can have major influence at the regional scale. Many of them are however themselves modulated by the ENSO, which remains the main quasi-global mode of variability observed at the annual to decadal timescales. Moreover, an original method has been here proposed to look for a better surrogate of climate change than ENSO variability. It consists of isolating a subset of individual years in the coupled integrations, where the interannual variability of tropical SST resembles the patterns of the tropical SST response to global warming. Such a stratification of the simulated timeseries can be used to isolate the impact of changes in the large-scale tropical circulation (related to the tropical SST pattern of climate change) from a residual impact that is difficult to interpret but is useful to understand the contrasted GLP sensitivity between the different models. Unfortunately, it is not possible to do the stratification for all models since they can exhibit very different tropical SST patterns at the interannual versus climate change timescale.

While our results suggest that the strong GLP sensitivity to global warming found in the NCAR scenario,

Fig. 13 Same as Fig. 4, but the whole GLP and global temperature anomaly distributions are now split in three samples corresponding to the lower (*blue*), upper (*red*) and remaining (*green*) quintiles of the ACC distribution measuring the similarity between detrended annual mean tropical SST anomalies and the SST patterns of climate change. Linear fits are estimated for the whole distribution (*black line*) and for the lower and upper quintiles (blue and red lines respectively)

and in the CCCMA scenario before 2050 (Fig. 2), should be considered very cautiously given the lack of ability of these models to capture the ENSO–GLP teleconnection, this ability remains a limited constraint on the global hydrological response in the SRES-A2 IPCC scenarios. Actually, it is still unclear whether the low sensitivity of the CGU models is more credible than the medium sensitivity of the CNRM, MPI and MRI models. Nevertheless, looking at the interannual climate variability provides some explanations to the model spread. It is not only the present-day ENSO–GLP relationship that exerts a major influence on the tropical hydrological response to global warming, but also a possible modulation of this relationship during the twenty-first century. Such an impact appears in several models and generally (though not necessarily) shows a weakening of the ENSO-tropical rainfall teleconnections. The various scenarios based on the CNRM model suggest however that this effect might occur only in the most extreme scenarios.

A possible continuation of this study would be to better understand the physical and dynamical mechanisms that control the ENSO variability in each model.

This "microscopic" rather than "macroscopic" approach would be very helpful to detect the models that shows a realistic behaviour for bad rather than good reasons. In particular, attention should be paid to the role of the large-scale circulation as a driving belt between tropical SSTs and precipitation anomalies. In the future, more sophisticated statistical tools, such as those used in detection studies, will also be necessary to better constrain the global hydrological response in the IPCC scenarios. Moreover, satellite measurements of oceanic precipitation should be operated continuously to provide a better picture of the observed precipitation change. Besides annual means, changes in seasonal and/ or extreme precipitation should be also explored. Regional scale detection studies are also needed given the heterogeneous spatial distribution of model uncertainties. This last remark is clearly illustrated by Fig. 14, zooming in on the twenty-first century precipitation change simulated over southern Europe and northern Africa in the eight SRES-A2 scenarios analysed in the present study. While all models indicate a dipolar response over Europe, very contrasted regional anomalies are simulated over West Africa, which remains one
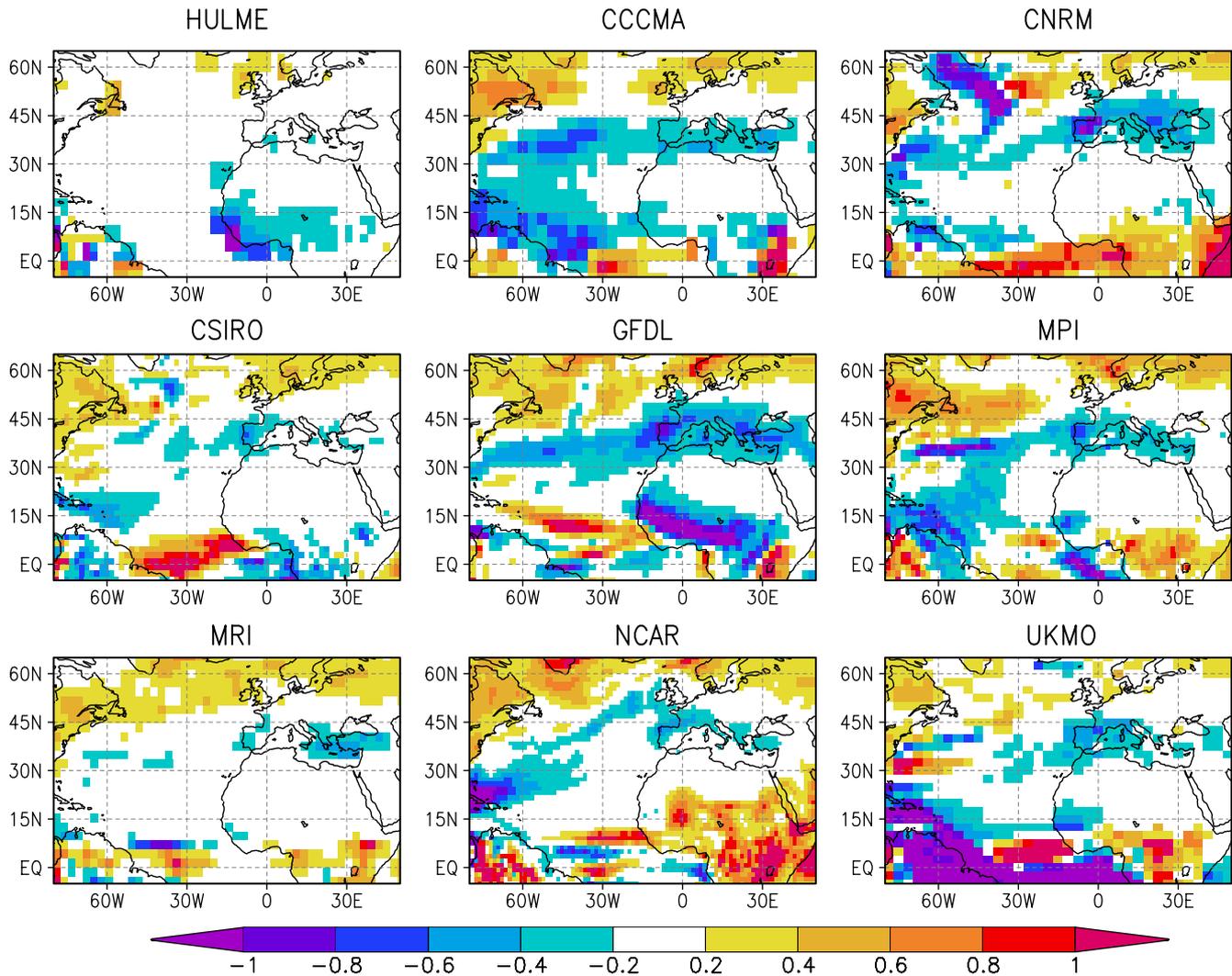
Fig. 14 Same as Fig. 12, but zooming over southern Europe and northern Africa

of the regions where the anticipation of climate change is particularly urgent given the obvious difficulties in implementing mitigation policies in developing countries.

References

Adler et al (2003) The version 2 Global Precipitation Climatology Project (GPCP) monthly precipitation analysis (1979-present). J Hydrometeor 4:1147–1167

Allen MR, Ingram WJ (2002) Constraints on future changes in climate and the hydrological cycle. Nature 419:224–232

Ashrit RG, Douville H, Rupa Kumar K (2003) Response of the Indian monsoon and ENSO-monsoon teleconnection to enhanced greenhouse effect in the CNRM coupled model. J Meteor Soc Jpn 81:779–803

Bosilovich MG, Schubert SD, Walker GK (2005) Global changes of the water cycle intensity. J Clim 18:1591–1608

Brooks N (2004) Drought in the African Sahel: long term perspectives and future prospects. Tyndall Centre working paper no 61: 31pp

Camberlin P, Zhao Y, Chauvin F, Douville H (2004) Simulated ENSO-tropical rainfall teleconnections as from the ARPEGE-OPA coupled ocean-atmosphere model. Climate Dyn 23:641–657

Diaz HF, Hoerling MP, Eischeid JK (2001) ENSO variability, teleconnections and climate change. Int J Climatol 21:1845–1862

Douville H, Royer J-F, Polcher J, Cox P, Gedney N, Stephenson DB, Valdes PJ (2000) Impact of CO2 doubling on the Asian summer monsoon: robust versus model dependent responses. J Meteorol Soc Jpn 78:1–19

Douville H, Chauvin F, Planton S, Royer J-F, Salas Mélia D, Tyteca S (2002) Sensitivity of the hydrological cycle to increasing amounts of greenhouse gases and aerosols. Climate Dyn 20:45–68

Douville H (2005) Impact of regional SST anomalies on the Indian monsoon response to global warming in the CNRM climate model. J Climate (revised)

Gershunov A, Barnett T (1998) Inter-decadal modulation of ENSO teleconnections. BAMS 79:2715–2725

Gershunov A, Schneider N, Barnett T (2001) Low-frequency modulation of the ENSO-Indian monsoon rainfall relationship: signal or noise? J Clim 14:2486–2492

Hulme M, Osborn TJ, Johns TC (1998) Precipitation sensitivity to global warming: comparison of observations with HadCM2 simulations. Geophys Res Lett 25:3379–3382

IPCC (2001) Climate change 2001: the scientific basis. In: Houghton JT et al (eds) Cambridge University Press, Cambridge

Jancovici J-M (2004) Energy and climate change: discussing two opposite evolutions. J de Phys (Proce) 121:171–184

Kumar A, Yang F, Goddard L, Schubert S (2004) Differing trends in the tropical surface temperatures and precipitation over land and oceans. J Clim 17:653–664

Lau KM, Ho CH, Chou MD (1996) Water vapor and cloud feedback over the tropical oceans: Can we use ENSO as a surrogate for climate change? Geophys Res Lett 23:2971–2974

Liepert BG, Feichter J, Lohmann U, Roeckner E (2004) Can aerosols spin down the water cycle in a warmer and moister world? Geophys Res Lett 31: doi:10.1029/2003GL019060

Murphy JM, Sexton DMH, Barnett DN, Jones GS, Webb MJ, Collins M, Stainforth DA (2004) Quantification of modelling uncertainties in a large ensemble of climate change simulations. Nature 430:768–772

Rayner NA, Parker DE, Horton EB, Folland CK, Alexander LV, Rowell DP, Kent EC, Kaplan A (2003) Global analyses of sea surface temperature, sea ice and night maritime air temperature since the late nineteenth century. J Geophys Res 108: doi:10.1029/2002JD002670

Soden BJ (2000) The sensitivity of the tropical hydrological cycle to ENSO. J Clim 13:538–549

Timmerman A, Oberhuber J, Bacher A, Esch M, Latif M, Roeckner E (1999) Increased El Niño frequency in a climate model forced by future greenhouse warming. Nature 398:694–697

Yang F, Kumar A, Schlesinger ME, Wang W (2003) Intensity of hydrological cycles in warmer climates. J Clim 16:2419–2423